

# Annual Report, 1999

## Simulation of Ground Motion in the Los Angeles Basin

Yuehua Zeng and John Anderson  
Seismological Laboratory and Department of Geological Science  
Mackay School of Mines, University of Nevada - Reno

### Progress Report

Over the past several years, we have developed theories and methods for modeling synthetic strong ground motion using a composite source model (Zeng et al., 1994). This year we have used the composite source model to determine fault rupture processes for several important earthquakes in California and Kobe, Japan, and to investigate their source characteristics on near field ground motions. We also participated in the emergency response to the Chi Chi, Taiwan earthquake to study the strong motion data from this large thrusting event. Our results are summarized below.

Using the Genetic Algorithm inversion, we inverted the strong motion data to obtain the composite earthquake source rupture processes. The velocity seismograms of those earthquakes were filtered with a pass band specified between 8 to 0.7 second period. For every earthquake events, their regional velocity structures were modified to add a 30 meters low velocity layer and a 100 meters transition layer on top of those velocity models to accommodate the site condition at each station. The average shear wave velocity of the top 30 meters layer is assigned according to the USGS published site classification using shear wave velocities.

We first studied the Imperial Valley earthquake source rupture process. A total of 28 stations were selected for the source inversion. Figure 1a shows a map view of the station and fault geometry distribution. We used the same fault geometry and seismic moment as that of Hartzell and Heaton (1983). Figure 1b shows the slip distribution of this earthquake plotted in both slip vector and amplitude intensity scale. We found one large slip zone in the center on the fault. The result is consistent with the solution obtained by Hartzell using teleseismic and strong motion observation. The lack of slip near the hypocenter indicates that the earthquake started with a weak asperity. The rupture was then accelerated from the hypocenter northward. Hartzell and Heaton have suggested that the large slip in the middle of the fault could be a triggered event by a smaller rupture event near the hypocenter.

For the Loma Prieta earthquake, we have selected a total of 34 for the waveform inversion to find a specific composite source model of this event (Figure 2a). The seismic moment of this earthquake is estimated at  $2.9 \times 10^{26}$  dyne-cm. Figure 2b plots the slip distribution in vector and amplitude intensity scale. The result shows a large slip source located on the southeast side of the fault and another large slip source on the northwest side of the fault. Slip orientation changes from pure strike slip on the southeast side of the fault to oblique slip on the northwest side of the rupture plane. This solution agrees very well with Wald et al. (1991) using an entirely different inversion technique.

The 28 June 1992 Landers earthquake (Mw 7.2) ruptured through the fault of 70 km with a source duration of around 24 second. A map view of the fault geometry and selected strong motion station distribution is shown in Figure 3a. A total of 13 stations were used for the inversion. The seismic moment of this event is estimated to be  $7.7 \times 10^{26}$  dyn-cm. Figure 3b plots the distribution of slip vector and amplitude over the fault plane. Our inversion solution differs from Wald et al. (1994) and shows large slip zones near the centers of the three fault segments. Location of minimum fault slips coincide well with the ends or stepping sections of the fault, suggesting that fault stepovers act like barriers to the source dynamic rupture.

Zeng and Anderson (1996) have studied the Northridge earthquake rupture process using the Genetic Algorithm and the composite source model. This study differs from the previous investigation by using a variable rake for the fault slip and a total of 33 strong motion records instead of a constant rake and a total of 10 seismograms. We used the same fault geometry as that of Wald et al. (1996) for comparison. The seismic moment of this earthquake is estimated to be  $1.4 \times 10^{26}$  dyne-cm. Figure 4a shows a map view of the station and fault geometry distribution. The earthquake slip intensity and slip vector distribution over the fault plane were plotted in Figure 4b. The result indicates a complex earthquake rupture process with three large slip zones: one above the hypocenter, and two others located to the west of the hypocenter.

Near fault strong motion records of the January 17, 1995 Kobe, Japan earthquake were also used to study the rupture process of this event. A total of 15 strong motion seismograms within about 30 km of the fault were selected (Figure 5a). We used the same fault geometry of Wald (1996). The moment of the earthquake is estimated about  $2.4 \times 10^{24}$  dyne-cm. Figure 5b shows the resulting slip and rake distribution of the composite source model determined from the waveform inversion. The plot suggests that much of the earthquake moment was released at shallow depths of the first fault segment. However, the smaller slip sources from the second fault segment actually causes more damage to the surface structures.

With the earthquake source model derived above, we then test the effect of rupture directivity of the composite source model comparing with the observation. Our error analysis shows the composite source model simulations are consistent with the observed directivity effects. We did not find any significant bias trends in terms of the weighted cross-correlation and response spectrum ratios between synthetics and observations.

For the Chi Chi, Taiwan, earthquake of magnitude 7.6, the fault dimension was determined using the surface rupture data of the Taiwan Geological Survey and the aftershock distribution. The fault was divided into four segments along strike with a total length of 80 km to approximate the surface rupture observation. The fault width was assumed to be 40 km. We used the seismic moment and focal mechanism of USGS as our start model. The velocity structure of the region was determined using the surface wave modeling result of Chen et al. (1998). Our preliminary analysis indicates two large slip zones on the fault, one located below the hypocenter at a depth of 15 km and the other larger asperity located 30 km north of the hypocenter at a depth of 10 km. Most of the moment release occurred on the northern part of the rupture plane (Figure 6). Rupture at the southern end of the fault plane has a slight right

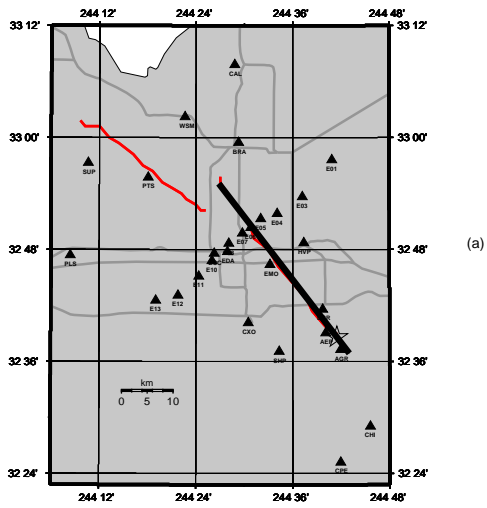
lateral slip component. At the northern end of the plane, rupture occurred as a pure thrust slip. For most part of the fault the rupture has a left lateral slip component.

## References

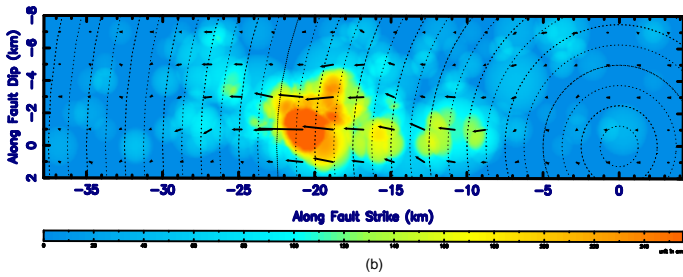
- Chen, C.-H., T.-L. Teng and Y.-C. Gung (1998). Ten-second Love wave propagation and strong ground motions in Taiwan, *J. Geophys. Res.*, 103, p21,253-21,273.
- Hartzell, S. H. and T. H. Heaton (1983). Inversion of strong ground motion and teleseismic waveform data for the fault rupture history of the 1979 Imperial Valley, California, earthquake, *Bull. Seism. Soc. Am.* No. 73, 6, 1553-1583.
- Wald, D. J., T. H. Heaton, and D. V. Helmberger, (1991), Rupture model of the 1989 Loma Prieta earthquake from the inversion of strong motion and broadband teleseismic data, *Bull. Seism. Soc. Am.*, 81, 1540-1572, 1991.
- Wald, D. J., and T. H. Heaton (1994), Spatial and temporal distribution of slip for the 1992 Landers, California, earthquake, *Bull. Seism. Soc. Am.*, 84, 668-691, 1994.
- Wald, D. J., T. H. Heaton, and K. W. Hudnut (1996). The slip history of the 1994 Northridge, California, earthquake determined from strong-motion, teleseismic, GPS, and Leveling data, *BSSA*, 86, S49-S70.
- Wald, D. J. (1996). Slip history of the 1995 Kobe, Japan, earthquake determined from strong ground motions, teleseismic, geodetic data, *J. Physics of the Earth*, 44, 489-504.
- Zeng, Y., J. G. Anderson and G. Yu (1994). A composite source model for computing realistic synthetic strong ground motions, *J. Res. Lett.*, **21**, 725-728.
- Zeng, Y. and J. G. Anderson (1996). A composite source modeling of the 1994 North-ridge earthquake using Genetic Algorithm, *Bull. Seism. Soc. Am.* 86, No. 1B, 71-83.

## Publication List

- Zeng, Y. (1999). Source modeling and directivity study of the Loma Prieta and several other large earthquake, *EOS, Trans. A.G.U.*, **80**, F40.
- Chen, C.-H. and Y. Zeng (1999). Inversion of the source rupture process of the September 20, 1999 Chi Chi, Taiwan, earthquake, Fall AGU Meeting Program, p12.
- Lee, Y., J. G. Anderson and Y. Zeng (1999). Evaluation of empirical attenuation relations, submitted to *Bull. Seis. Soc. Am.*
- Ni, S.-D., J. G. Anderson, Y. Zeng, Raj V. Siddharthan (1999). Expected signature of nonlinearity on regression for strong ground motion parameters, revised to *Bull. Seis. Soc. Am.*

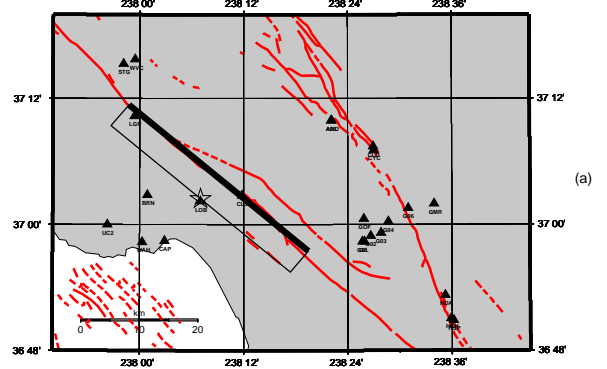


Slip Amplitude Distribution of the Imperial Valley Earthquake

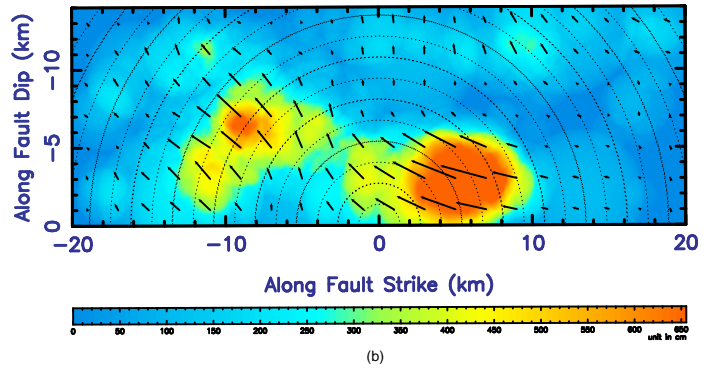


(b)

Figure 1. (a) Fault geometry and stations distribution. (b) Slip distribution of the composite source model.

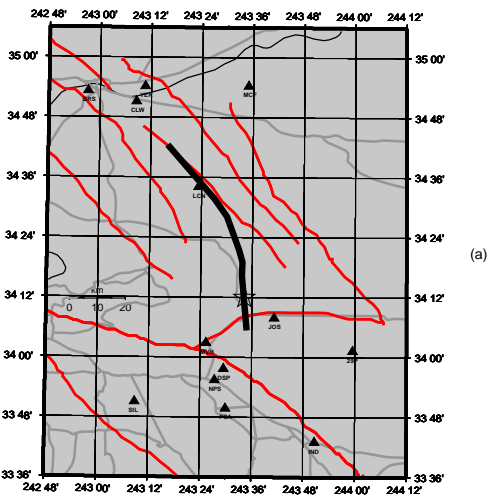


Slip Amplitude Distribution of the Loma Prieta Earthquake

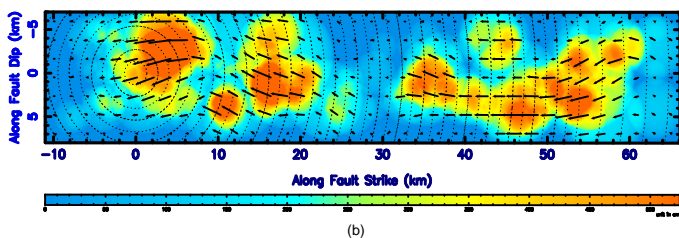


(b)

Figure 2. (a) Fault geometry and stations distribution. (b) Slip distribution of the composite source model.

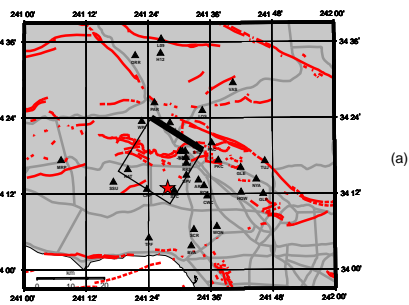


Slip Amplitude Distribution of the Landers Earthquake

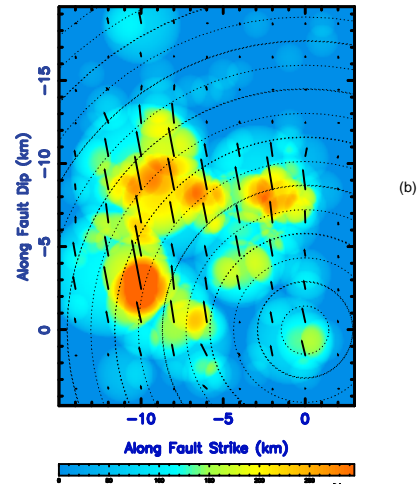


(b)

Figure 3. (a) Fault geometry and stations distribution. (b) Slip distribution of the composite source model.

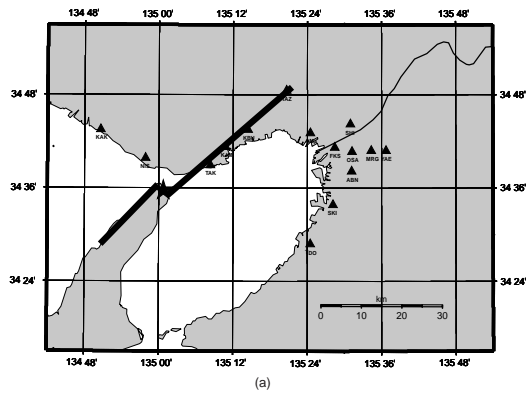


Slip amplitude distribution for the Northridge earthquake



(b)

Figure 4. (a) Fault geometry and stations distribution. (b) Slip distribution of the composite source model.



Slip Amplitude Distribution for the Kobe Earthquake, Japan

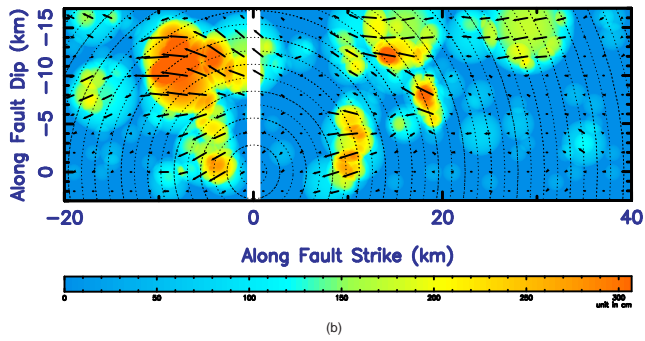
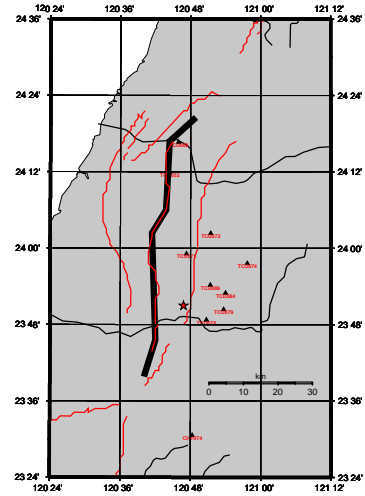


Figure 5. (a) Map view of the Kobe earthquake fault geometry and strong motion station distribution. (b) Slip distribution of the composite source model for the Kobe earthquake obtained from waveform fitting between the observed and synthetic strong motion seismograms.



Slip Amplitude Distribution of the Chi Chi earthquake

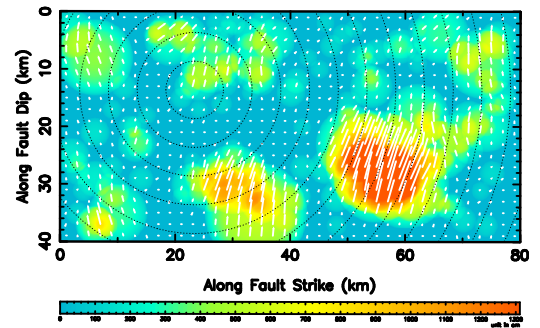


Figure 6. (a) Fault geometry and station distribution for Chi Chi Taiwan earthquake. (b) Slip amplitude intensity and vector distribution of the composite source model.